CHEMISTRY OF MATERIALS

pubs.acs.org/cm Article

Unraveling the Origin of Moisture Stability of Halide Solid-State Electrolytes by *In Situ* and *Operando* Synchrotron X-ray Analytical Techniques

Weihan Li,[#] Jianwen Liang,[#] Minsi Li,[#] Keegan R. Adair, Xiaona Li, Yongfeng Hu, Qunfeng Xiao, Renfei Feng, Ruying Li, Li Zhang, Shigang Lu, Huan Huang, Shangqian Zhao,* Tsun-Kong Sham,* and Xueliang Sun*

Cite This: *Chem. Mater.* 2020, 32, 7019−7027 Read Online

ABSTRACT: Recently, halide solid-state electrolytes (SSEs) have been reported to exhibit high ionic conductivity and good compatibility with cathode materials. However, the air stability of halide-based electrolytes is one important factor related to ionic conductivity upon exposure to air for practical applications. The instability mechanism of Li_3InCl_6 toward air is not clearly understood. Herein, we for the first time report the application of *operando* optical microscopy, Raman spectroscopy, synchrotron-based X-ray powder diffraction, and *in situ* X-ray absorption near-edge structure for the study of halide electrolyte air stability. Using these methods, we have been able to track the degradation process of Li_3InCl_6 exposed to air. It is for the first time found that Li_3InCl_6 is hydrophilic in character, leading to the absorption of moisture from the air, and a portion of Li_3InCl_6 reacts with absorbed H_2O to form In_2O_3, LiCl, and HCl. Moreover, the remaining electrolyte absorbs H_2O to form a hydrate, $Li_3InCl_6{\cdot}xH_2O$. The reaction results in a decrease of ionic conductivity. Additionally, the influence of air stability on the practical application of Li_3InCl_6 has been explored. Li_3InCl_6 shows much better stability against air with low humidity (3%) and in battery dry rooms, making it a promising SSE for application in the commercial lithium-ion manufacturing industry.

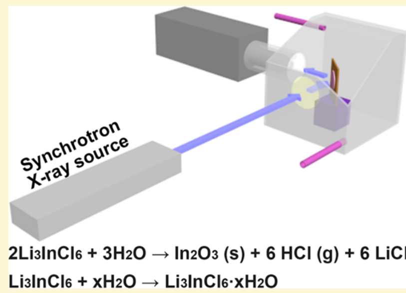

■ INTRODUCTION

Recently, all-solid-state lithium-ion batteries (ASSLIBs) have attracted intensive research interest owing to their high theoretical energy density and improved safety. Compared with traditional lithium-ion batteries (LIBs), ASSLIBs use solid-state electrolytes (SSEs) as the lithium-ion transport media, which can, in principle, overcome the safety issues in LIBs associated with the use of liquid electrolytes (*e.g.* flammability and lithium dendrite growth). Additionally, ASSLIBs can potentially increase the energy density of the system through using high-voltage cathodes and lithium metal anodes, which cannot be directly used in liquid electrolyte-based LIBs.[1−3] Until now, several types of SSEs have been developed. Among them, sulfide and oxide SSEs, such as $Li_{10}GeP_2S_{12}$ (LGPS), $Li_7P_3S_{11}$ (LPS), and garnets, show high ionic conductivity (*e.g.* 10^{-2} to 10^{-3} S cm^{-1}) and potential for practical applications.[4−8] However, these two types of SSEs face several challenges, such as narrow electrochemical stability windows, serious interfacial reactions between sulfide electrolytes and electrode materials, and the complicated fabrication process of oxide garnets (*e.g.* high-temperature annealing).[9,10]

To overcome these issues, halide-based SSEs (*i.e.* Li_3YCl_6 and Li_3YBr_6) have been recently reported by Asano *et al.* and show high ionic conductivity (10^{-3} S cm^{-1}) at room temperature along with good compatibility with $LiCoO_2$ cathode materials.[11] More recently, our group reported another promising halide SSE, Li_3InCl_6, which shows high ionic conductivity (>10^{-3} S cm^{-1}) and good compatibility with $LiCoO_2$ and $LiNi_{0.8}Co_{0.1}Mn_{0.1}O_2$ cathode materials.[12,13] Mo *et al.* provided a detailed understanding of these two halides and predicted other promising halide SSEs with high ionic conductivity and wide electrochemical stability windows through first-principles calculations.[14] However, for practical applications, the air stability of SSEs is another important factor needing evaluation, in addition to ionic conductivity and compatibility.[3,15] Our previous works show the reduction of ionic conductivity of Li_3InCl_6 upon exposure to ambient air.[12,13] In addition to Li_3InCl_6, Li_3YCl_6 has also been found to be unstable when exposed to ambient air. In previous studies, halide SSEs were reported to be stable against dry air or oxygen, which indicates that moisture can react with halides

Received: June 9, 2020
Revised: July 22, 2020
Published: July 23, 2020

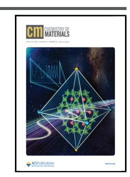

https://dx.doi.org/10.1021/acs.chemmater.0c02419
Chem. Mater. 2020, 32, 7019−7027

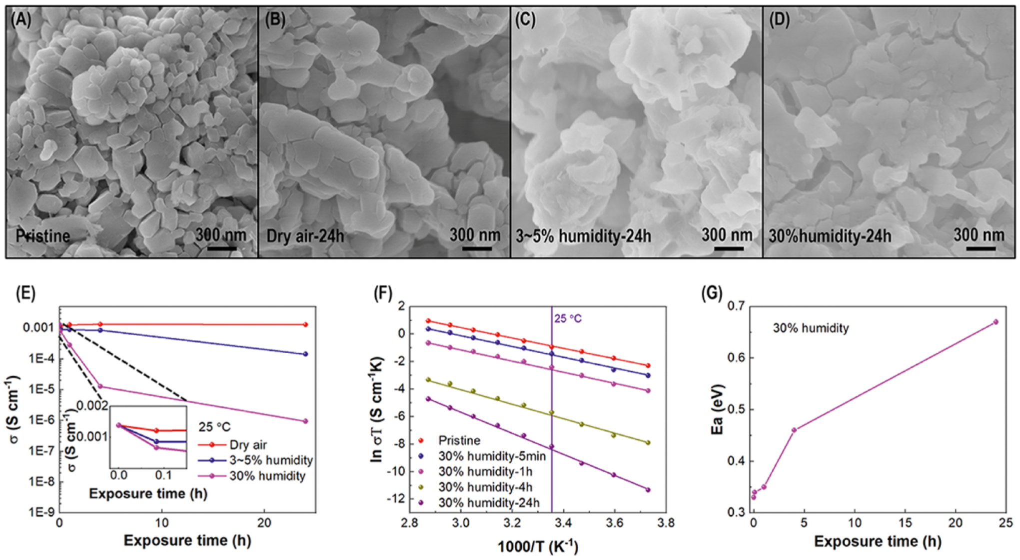

Figure 1. SEM images of (A) pristine Li_3InCl_6 and (B–D) Li_3InCl_6 when exposed to air with different degrees of humidity (*i.e.* 0% as dry air, 3–5% humidity and 30% humidity) for 24 h. (E) The Li-ion conductivity evolution at 25 °C of Li_3InCl_6 when exposed to air with different levels of humidity (*i.e.* dry air, 3–5% humidity and 30% humidity) (F) Arrhenius plots and (G) activation energy of Li_3InCl_6 when exposed to air with 30% humidity for different time intervals.

upon exposure to ambient air.[11] However, the reaction mechanism between halides and ambient air remains elusive. Therefore, it is of importance to understand what happens to halides upon exposure to ambient air and then find out reasonable methods to prevent degradation. Until now, several works have reported chemical degradation of sulfides and oxides in ambient air.[16−18] Oxides react with moisture and CO_2 in the air to form Li_2O, LiOH, and Li_2CO_3, and the resultant impurities lead to a reduction in ionic conductivity.[16,18] In the case of sulfides, H_2S gas is generated owing to the reaction with moisture in air, leading to significant structural change.[17] However, to the best of our knowledge, there is no work on the detailed study of air stability of halide electrolytes. Even in the previous air stability studies of oxides and sulfides, several issues have not been clarified because of the limitations of characterization methods. In principle, while X-ray powder diffraction (XRD) can be used to determine the evolution of crystal phases in SSEs upon exposure to air, it cannot track the local structure of amorphous phases. Raman spectroscopy is typically used to identify the molecules *via* functional group vibrational frequencies and lattice modes, but it cannot adequately track the reaction of SSEs upon exposure to air, as shown previously.[17] Additionally, the *ex situ* XRD or Raman studies on air stability used in the previous work lack the capabilities to track metastable phases formed upon the exposure to air.[19]

To overcome the challenges in the air stability study of halide SSEs, we carried out *operando* optical microscopy, Raman spectroscopy, synchrotron-based XRD (SXRD), and *in situ* X-ray absorption near-edge structure (XANES) studies, which allow the reaction to be tracked in real time with the crystal structure and chemical resolution.[20−22] The use of different types of *in situ* and *operando* characterization methods realizes the real-time detection of the degradation process of halide SSEs in terms of macroscale digital photos, crystal structures, nanoscale molecular level, and local chemical environment at the atomic level. Through studying the air stability of Li_3InCl_6 halide SSEs, a clear picture of the degradation of Li_3InCl_6 in air has emerged.

EXPERIMENTAL SECTIONS

Characterizations. XRD patterns were collected on a Bruker AXS D8 ADVANCE with Cu Kα radiation (λ = 1.54178 Å) with a special holder to avoid exposure to air during the test. *Ex situ* and *operando* optical microscopy and Raman spectroscopy were carried out using a HORIBA Scientific LabRAM HR Raman spectrometer system equipped with a 532.4 nm laser.

Ionic Conductivity Measurements. Ionic conductivities of Li_3InCl_6 and air treated samples were measured by alternating current (AC) impedance spectroscopy. Typically, powder samples were placed between two stainless steel rods with 10 mm diameter and pressed at 3 ton (∼380 MPa). The thickness of the pellet was between 0.8 and1.0 mm depending on the amount of powder sample used. The procedures were performed inside an Ar-filled glove box. Electrochemical impedance spectroscopy was performed with in the temperature range −5 to 75 °C using a versatile multichannel potentiostat 3/Z (VMP3) from 7 MHz to 1 Hz with an amplitude of 10 mV.

Synchrotron-Based XRD and XANES. Synchrotron-based X-ray powder diffraction was carried out at the very sensitive elemental and structural probe employing radiation from a synchrotron (VESPERS) beamline at the Canadian Light Source. The photon energy of incident X-ray was selected as 12 keV. The Li K-edge and In L_3- and Cl K-edge XANES spectra were collected using the variable line spacing plane grating monochromator (VLS-PGM) beamline and soft X-ray microcharacterization beamline (SXRMB), respectively at the Canadian Light Source. The X-ray fluorescence yield (FLY) mode was used to collect the XANES spectra. For the *in situ* In L_3- and Cl K-edge XANES study at the SXRMB beamline, a controlled chamber under He was used to realize the gas environment control.

RESULTS AND DISCUSSION

Morphology Change and Ionic Conductivity. Li_3InCl_6 SSE powder was prepared following the method reported in our previous work.[13] The synthesized SSE powder presents the typical XRD of Li_3InCl_6 (see Supporting Information, Figure S1A) and indicates a good crystalline structure. Lithium-ion conductivity was evaluated by the AC impedance method with

https://dx.doi.org/10.1021/acs.chemmater.0c02419
Chem. Mater. 2020, 32, 7019−7027

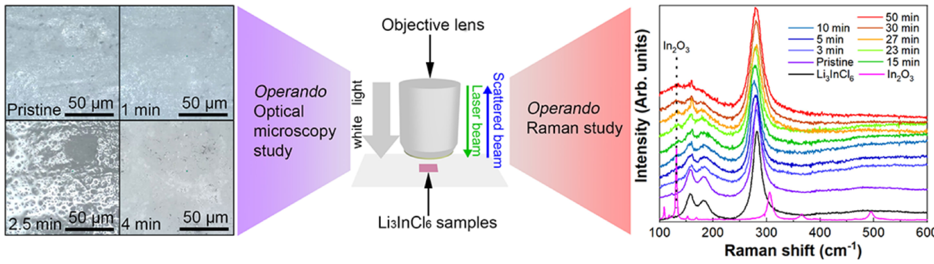

Figure 2. Schematic illustration (middle) of the *operando* optical microscopy and Raman spectroscopy setup. The Raman spectra evolution of Li_3InCl_6 when exposed to air with 30% humidity (right) and the *operando* optical microscopy images observed at different exposure times (left).

cold-pressed pellets. As shown in Figure S1B, the Arrhenius plot displays the relationship between the ionic conductivity and temperature. The ionic conductivity at 25 °C is 1.31×10^{-3} S cm^{-1}, which is comparable to the previously reported result.[13]

The influence of air on the morphology and ionic conductivity was first clarified. Figure 1A displays the scanning electron microscopy (SEM) image of pristine Li_3InCl_6, showing a typical polyhedron morphology with clear edges in the primary particles, which aggregate together and form larger secondary particles. The morphology change after exposure to air with different degrees of humidity (*i.e.* 0% humidity, 3−5% humidity and 30% humidity) is shown in Figures 1B−D and S2 (see Supporting Information). In the case of dry air, Li_3InCl_6 shows almost no change in the morphology after exposure for 24 h. However, 3−5% humidity and 30% humidity reveal a more serious impact on the morphology of Li_3InCl_6. When present in a humid environment, the clear edges of the primary particles disappear, and the primary particles aggregate together and merge into larger secondary particles. Additionally, higher humidity (30%) accelerates this process compared with lower humidity environments (3−5%). Moreover, as shown in Figure 1E, the ionic conductivity (at 25 °C) evolution of Li_3InCl_6 after exposure to air with different degrees of humidity was tracked. For a 24 h exposure period to dry air, ionic conductivity does not show any obvious change, indicating that dry air has a negligible effect on Li_3InCl_6. When the humidity increases to 3−5%, Li_3InCl_6 shows a significant reduction in ionic conductivity from 1.31×10^{-3} to 1.41×10^{-4} S cm^{-1} after 24 h, with little reduction during the initial 4 h. After furthering increasing the humidity to 30%, the ionic conductivity undergoes rapid degradation, reducing to 2.8×10^{-4}, 1.27×10^{-5}, and 9.4×10^{-7} S cm^{-1} after 1, 4, and 24 h, respectively. It is apparent from the evolution of the ionic conductivities of the SSE exposed to 3−5% and 30% humidity that the rate of ionic conductivity reduction increases with the increasing humidity. Subsequently, the effect of air with 30% humidity on the lithium transport was studied in detail. Figure 1F shows the Arrhenius plots of Li_3InCl_6 exposure to air with 30% humidity for different periods of time. The ionic conductivity of Li_3InCl_6 in the temperature range from −5 to 75 °C displays a decrease with the increasing exposure time. Moreover, the activation energy values after different treatment times have been calculated and plotted in Figure 1G based on the Arrhenius equation

$$\sigma = \sigma_0 \exp(-E_a/k_B T)/T \quad (1)$$

where σ is the ionic conductivity, σ_0 is the prefactor, k_B is the Boltzmann constant, and E_a is the activation energy related to the barrier along the lithium-ion diffusion path.[23] Along with the increasing exposure time, E_a increases considerably from 0.33 eV in the pristine state to 0.67 eV after 24 h, showing that the Li-ion transport becomes more difficult and that new phases with much poorer ionic conductivity might form during the reaction. The evolution of ionic conductivity in Li_3InCl_6 exposed to air indicates that moisture plays a major role in the degradation of Li_3InCl_6. However, more evidence is required to confirm this notion.

***Operando* Optical Microscopy and Raman Spectroscopy Studies.** To confirm the reaction of Li_3InCl_6 upon exposure to air, *operando* optical microscopy and Raman spectroscopy were carried out in a 30% humidity environment to track the change of morphology and chemical composition, as shown in Figure 2. The optical microscopy images of the surface of Li_3InCl_6 reveal very quick morphological changes within several minutes, confirming the hydrophilic character of Li_3InCl_6. Then, *operando* Raman spectroscopy was used to detect the chemical reaction upon exposure. To realize high temporal resolution, the acquisition time for each spectrum was set to 1 min. The reference Raman spectrum of Li_3InCl_6 was collected using a thin microglass cover to avoid contact with air. In the case of the *operando* study, the pristine Raman spectrum is in good agreement with the reference spectrum, suggesting a minimal reaction at the beginning. During the exposure process, a series of Raman spectra were continuously collected as a function of time. Compared with the pristine spectrum, the Raman spectra underwent several obvious changes. Three typical peaks at 159, 184, and 280 cm^{-1} show a decrease in intensity and increase in width with increasing exposure time. Moreover, the two peaks at 159 and 184 cm^{-1} nearly disappear after 50 min, providing evidence that Li_3InCl_6 has partially degraded and becomes more disordered. Nevertheless, not all Li_3InCl_6 reacts with air. One of the products should be the hydrate of Li_3InCl_6, which will be discussed below with other characterization results (SXRD and XANES). Interestingly, a new peak around 131.5 cm^{-1} emerges upon exposure. Compared with several reference spectra of compounds containing Li, Cl, and In (see Supporting Information, Figure S3), this new peak can be attributed to In_2O_3, which should be one of the products formed during the reaction between Li_3InCl_6 and air. To further confirm the formation of O−H bonds, Figure S4 (see Supporting Information) shows the Raman spectra evolution of O−H stretching upon exposure to air with 30% humidity in a wavenumber range from 3000 to 3800 cm^{-1}.[24−26] The broad peaks between 3300 and 3600 cm^{-1} belonging to O−H stretching and the area of the peaks increase gradually with the exposure time. This finding indicates that Li_3InCl_6 absorbs moisture and results in the possible formation of the

https://dx.doi.org/10.1021/acs.chemmater.0c02419
Chem. Mater. 2020, 32, 7019−7027

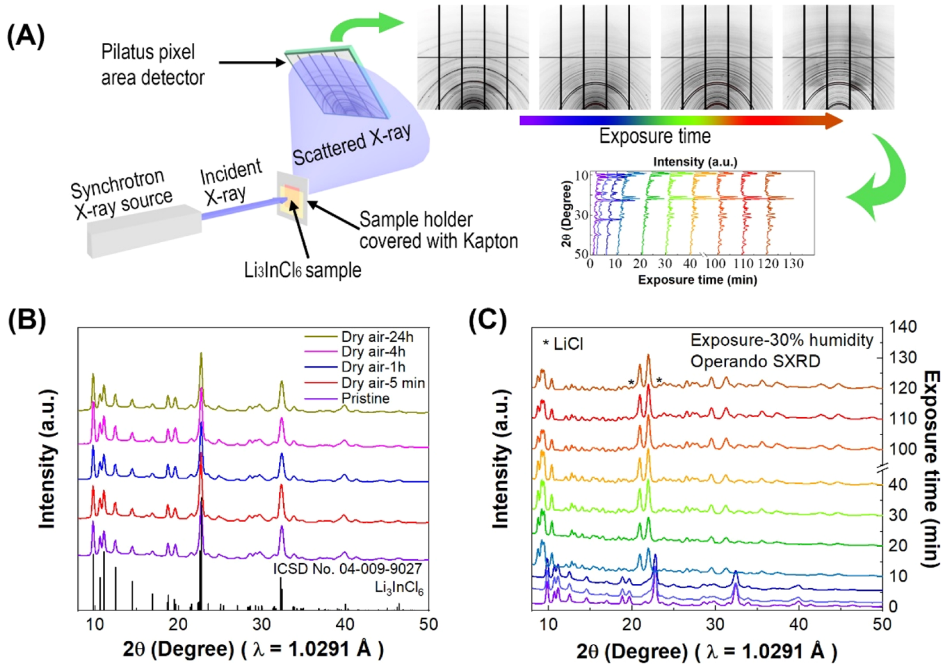

Figure 3. (A) Schematic illustration of the *operando* synchrotron-based X-ray powder diffraction (SXRD) study of Li_3InCl_6 when exposed to air with 30% humidity. (B) *Ex situ* SXRD patterns of Li_3InCl_6 exposed to dry air for different time intervals. (C) *Operando* SXRD patterns of Li_3InCl_6 during exposure process to air with 30% humidity for 120 min.

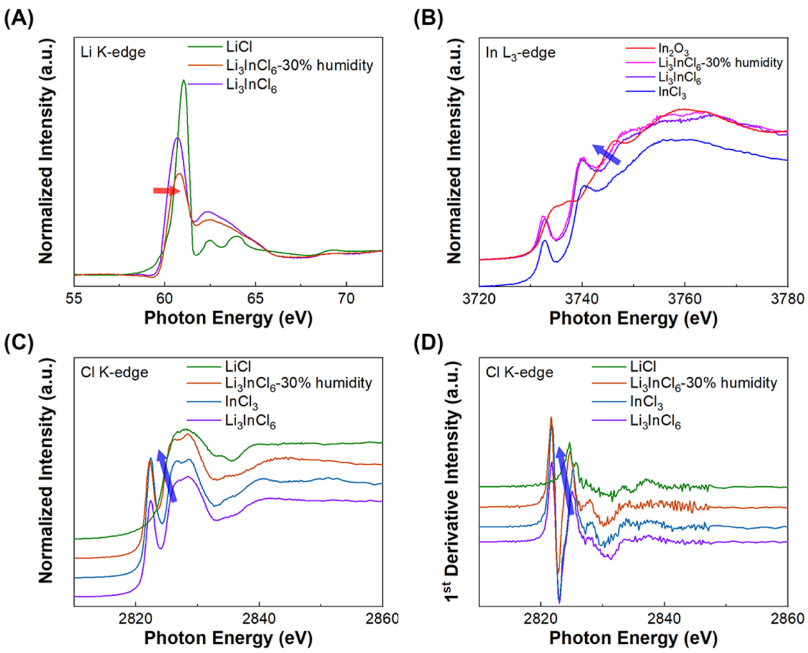

Figure 4. (A) Li K-edge, (B) In L_3-edge, and (C) Cl K-edge XANES spectra and (D) first derivate spectra of the Cl K-edge XANES comparing pristine Li_3InCl_6 and Li_3InCl_6 exposed to air with 30% humidity for 2 h.

corresponding hydrate upon exposure to air with 30% humidity.

***Ex Situ* and *Operando* SXRD Study.** To detect other products upon the exposure process, *operando* SXRD was conducted to track the evolution of the crystal structure. As shown in Figure 3A, X-rays with a wavelength of 1.0291 Å are used to obtained powder diffraction, and the scattered X-ray beams are recorded with a Pilatus pixel area sensitive detector. The experimental setup is presented in the Supporting Information (Figure S5). The high flux (10^9 to 10^{11} photons/s) of synchrotron-based X-rays and the two-dimensional (2D) detector allow the XRD pattern to be recorded in a short time. The collection time of one SXRD can be performed from several seconds to minutes, which is short compared with the exposure duration of interest. After mounting the sample on the sample holder, a series of 2D X-ray scattering images of Li_3InCl_6 are collected upon exposure. Figure 3B shows the *ex situ* SXRD study on the influence of dry air on Li_3InCl_6. The pristine Li_3InCl_6 shows the typical pattern consistent with the reference pattern (ICSD

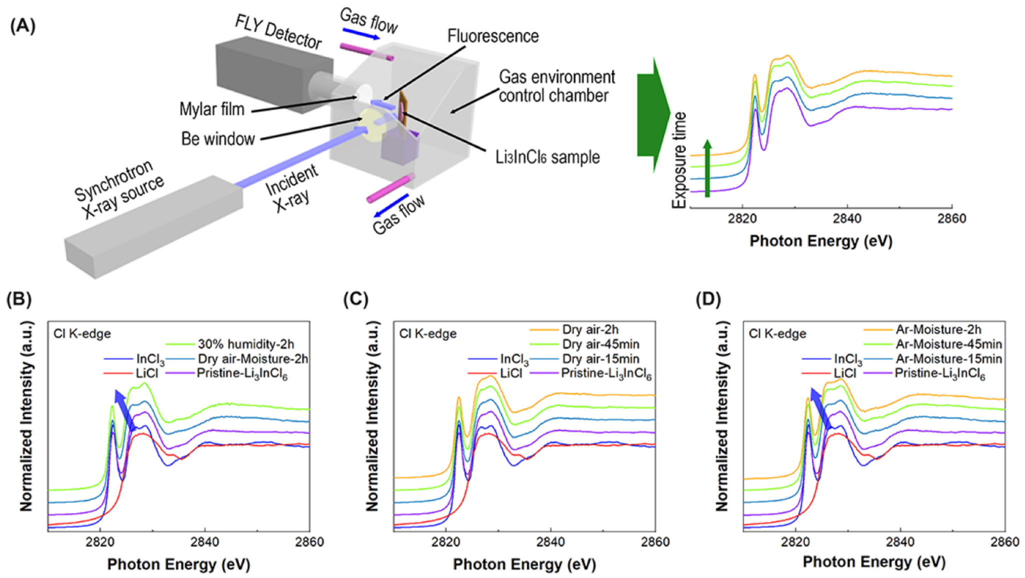

Figure 5. (A) Schematic illustration of *in situ* synchrotron-based XANES study of Li_3InCl_6 when exposed to three different gas environments (*i.e.* dry air, mixture of Ar and moisture, mixture of dry air and moisture). *In situ* Cl K-edge XANES studies of Li_3InCl_6 during exposure process to (B) the mixture of dry air and moisture, (C) dry air and (D) the mixture of Ar and moisture for 120 min.

no. 04-009-9027), confirming the distorted rock-salt LiCl structure with a good crystalline order. In the case of exposure to dry air, no change is found for the SXRD patterns compared with the pristine sample, indicating that Li_3InCl_6 is stable against dry air. These finding are in good agreement with the ionic conductivity results. Subsequently, the *operando* SXRD study was carried out by exposing Li_3InCl_6 to air with 30% humidity, as shown in Figure 3C. During the initial 5 min, the peak at 2θ = 22.8° gradually disappears. Then, after 10 min, the SXRD pattern changes significantly, and a new set of SXRD peaks appear, indicating that another crystal structure emerges at the expense of the original structure. As discussed in our recent results, the new set of SXRD peaks belong to $Li_3InCl_6{\cdot}xH_2O$.[12] In addition to the new set of peaks, the intensity of the two new peaks belonging to LiCl gradually increases with the exposure time. When the exposure time reaches 120 min, the SXRD pattern shows a mixture of a new set of peaks (2θ = ∼19.9 and ∼23.2°) belonging to $Li_3InCl_6{\cdot}xH_2O$ and LiCl, suggesting that both are the products of the reaction. The residual $Li_3InCl_6{\cdot}xH_2O$ in the final product confirms that not all of the Li_3InCl_6 react with air, as discussed above in the *operando* Raman spectroscopy study. To further confirm the lattice structure of $Li_3InCl_6{\cdot}xH_2O$, more characterization such as Rietveld refinement of SXRD with higher intensity and total scattering coupled with pair distribution function analysis should be used in the future.

***Ex Situ* and *Operando* XANES Spectroscopy Study.** Based on the *operando* Raman spectroscopy and SXRD studies, we have a good idea of the chemical composition of the final products resulting from exposure of Li_3InCl_6 to ambient moisture. Nevertheless, it remains unclear what gases in the air are responsible for the reaction with Li_3InCl_6. Hence, it is crucial to carry out *in situ* studies with exposure to several specific gases (*e.g.* dry air and moisture). The *in situ* synchrotron-based XANES spectroscopy makes it possible to track the change of the local chemical environment of elements in Li_3InCl_6 when exposed to different gas environments (see Supporting Information, Figure S6).

We first look at the *ex situ* XANES results. Figure 4 shows the Li K-edge, In L_3-edge, and Cl K-edge XANES spectra of pristine Li_3InCl_6 and Li_3InCl_6 exposed to air with 30% humidity for 2 h (denoted as Li_3InCl_6-30% humidity), which were collected using the FLY mode. Figure 4A shows the Li K-edge XANES spectra, which arise from the electron transitions from the Li 1s orbital to the unoccupied electronic states of the Li 2p character and reflect the lithium-atom surrounding environment.[27,28] Compared with pristine Li_3InCl_6, Li_3InCl_6-30% humidity shows a shift of the absorption edge to higher photon energy, which is similar to the reference LiCl Li K-edge XANES. This suggests that the local chemical environment surrounding element Li ions changes to an environment similar to LiCl, which is consistent with the formation of LiCl confirmed by the *operando* SXRD result. The In L_3-edge XANES spectra are displayed in Figure 4B, which is related to the electron transition from In $2p_{3/2}$ to uncopied s and d orbitals.[29] The In L_3-edge XANES spectrum of Li_3InCl_6 is very similar to that of $InCl_3$ and contains similar features, including the peaks at 3732.7 and 3740 eV. This indicates that the local environment of In is similar to that of In atoms in $InCl_3$ with In^{3+} occupying the octahedral sites surrounded by six Cl^-.[12] After exposing to air with 30% humidity, the XANES spectra show shift of the edge threshold to lower photon energy in Li_3InCl_6 30% humidity. This shift can be assigned to the chemical environment change from the octahedral sites of In^{3+} in Li_3InCl_6 to that in In_2O_3 surrounded by O^{2-}.[30] The surrounding chemical environment of Cl^- is also studied using Cl K-edge XANES, as shown in Figure 4C. Both pristine Li_3InCl_6 and $InCl_3$ show main absorption edges with the white line peak at ∼2826.8 and ∼2828.6 eV, respectively, which is attributed to the electron transition from the 1s orbitals to 4p orbitals. The same features are also presented in LiCl. However, the pre-edge peaked at ∼2822.4 eV is found for both pristine Li_3InCl_6 and $InCl_3$, which is absent in LiCl. This pre-edge feature is due to increase in covalency arising from the mixing of Cl p-orbitals (3p) with metal (*i.e.* In) d-orbitals in Li_3InCl_6 and $InCl_3$, which is not available in LiCl. This orbital hybridization allows the electron transition from Cl 1s

https://dx.doi.org/10.1021/acs.chemmater.0c02419
Chem. Mater. 2020, 32, 7019−7027

orbitals to the mixed orbitals, as the 1s → 3d transition of Cl in LiCl is forbidden.[31,32] The main absorption edge in the Cl K-edge XANES of Li_3InCl_6-30% humidity shifts to lower photon energy, almost overlapping with that of LiCl. This absorption edge shift is much clearly presented in the corresponding first derivatives, as shown in Figure 4D. The absorption edge position of pristine Li_3InCl_6 moves from 2825.2 eV (the same position for $InCl_3$) to 2824.5 eV (the same position for LiCl). This observation suggests that the local environment surrounding Cl^- changes from the $InCl_3$-like structure to the LiCl-like structure, consistent with the local environment change of Li^+. Additionally, because the pristine Li_3InCl_6 and Li_3InCl_6-30% share the similar pre-peak of the Cl K-edge, indicating the formation of the hydrate of Li_3InCl_6, as discussed above. The *ex situ* XANES studies thus suggest that the final product includes LiCl and In_2O_3, which fits the conclusion obtained from *operando* Raman spectroscopy and SXRD studies.

We next performed *in situ* XANES studies using the *in situ* reaction chamber with a focus on the Cl K-edge and In L_3-edge. Figure 5A shows the schematic illustration of the experimental setup, including three key parts: the synchrotron X-ray beam, the FLY detector, and the *in situ* reaction chamber. The reaction chamber is sealed with a Be window and Mylar film when connected with the synchrotron X-ray chamber and the FLY detector. Li_3InCl_6 was mounted on the sample holder inside the reaction chamber, where three types of gas (*i.e.* dry air, mixture of Ar and moisture, and mixture of dry air and moisture) flow past the samples. To make sure the gas environment inside the *in situ* XANES study chamber is controllable, the pressure inside the chamber was kept positive during gas treatment processes. After exposing the sample to different gases for a controlled period of time (*e.g.* 15 min), the reaction chamber was purged with He gas for at least 10 min to remove all other gas (*i.e.* air, Ar, and moisture). After the purge process, the XANES data acquisition with the FLY mode was carried out to track the Cl K-edge and In L_3-edge XANES spectra evolution along with the exposure time. Figure 5B shows the influence of the mixed gases of dry air and moisture, where Li_3InCl_6 goes through the same Cl K-edge XANES evolution with the same absorption edge shift after 2 h treatment compared with the *ex situ* XANES result shown in Figure 4C. Additionally, the *in situ* In L_3-edge XANES study presents the same result with a spectra shift, as shown in Figure S7A (see Supporting Information). This confirms that the mixed gas leads to the same degradation result as the ambient air with 30% humidity. Then, the influence of dry air and moisture was separately studied. As shown in Figures 5C and S7B, no change occurs to the Cl K-edge and In L_3-edge XANES features during the 2 h exposure process with dry air, confirming that the local chemical environment surrounding In^{3+} and Cl^- in Li_3InCl_6 is stable, which is consistent with the ionic conductivity study (Figure 1E) and *ex situ* SXRD study results (Figure 3B). Finally, the moisture was separately introduced to evaluate its influence on the local chemical environment of Li_3InCl_6. Because Ar is an inert gas, it was chosen as the carrier gas for moisture to flow through the reaction chamber.[11] As shown in Figure 5D, after 15 min exposure, the main absorption edge of Cl in Li_3InCl_6 shifts to a lower energy. Moreover, the moisture treatment also leads to the shift of In L_3-edge XANES spectrum to lower energy, as shown in Figure S7C. The similar evolution of the XANES spectra suggests that moisture results in the same change of the local chemical environment surrounding In^{3+} and Cl^-, compared with the results observed when the electrolyte was exposed to air with 30% humidity. Based on these *in situ* and *ex situ* XANES study, it can be concluded that moisture is the reason that Li_3InCl_6 reacts and results in the degradation of ionic conductivity. Furthermore, the reaction products containing LiCl and In_2O_3 are identified.

Discussion of Air Stability of Li_3InCl_6. Taking the ionic conductivity, optical microscopy, Raman spectroscopy, SXRD, and XANES study results into account, the degradation of Li_3InCl_6 in ambient air is confirmed to be related to moisture. More importantly, Raman spectroscopy used a 532.4 nm (~2.3 eV) laser, which can get the chemical information at the surface. Cl K-and In L_3-edges XANES spectra were carried out using the synchrotron-based X-ray with the photon energy of several k eV, which can go beyond the surface with the probing depth of several micrometers, while SXRD was carried out using synchrotron-based X-ray with a photon energy of 12 keV, which can penetrate the overall samples and present the crystal structural information of the overall materials. Therefore, the combination of Raman spectroscopy, SXRD, and XANES studies presents the evolution of Li_3InCl_6 from the surface to the bulk material. To further confirm the previous characterizations, Li_3InCl_6 (20 wt %) was dissolved in deionized (DI) water, which was then used to study the reaction in the solution phase, as shown in Figure S8 (see Supporting Information). At the beginning, the solution was transparent without any precipitate with a pH value of around 4−5. Then, after storing for 24 h, some precipitate was found at the bottom of the flask, and the pH value decreased to around 3−4. Raman spectroscopy of the precipitate confirms that the product is In_2O_3. This means that the reaction between Li_3InCl_6 and DI water leads to the formation of In_2O_3 precipitate, which is insoluble in DI water, and the decrease of pH value is due to the formation of HCl. Because there is no obvious XRD peak, Raman and XANES spectra features belonging to other In-containing composites, such as InOCl or $Li_3InCl_{6-x}(OH)_x$, In_2O_3 should be the final product of the reaction. Moreover, the formation of H^+ is further confirmed by another dissolution experiment. As shown in Figure S9 (see Supporting Information), where Li_3InCl_6 was dissolved in a 2 M HCl solution with the same weight percentage (*i.e.* 20 wt %). Different from the solution using DI water as the solvent in Figure S8, this solution remains transparent, and there is no change of pH after being stored for 24 h. This suggests that the highly concentrated H^+ prevents the reaction between Li_3InCl_6 and H_2O to form HCl and In_2O_3, which should be one of the reaction products, based on Le Chatelier's principle. Based on the current characterization results, we propose that when Li_3InCl_6 is exposed to air, the moisture in the air is first absorbed by hydroscopic Li_3InCl_6. Following hydration, the absorbed water reacts with part of the halide to form In_2O_3 as the precipitate as well as LiCl and HCl. Moreover, residual Li_3InCl_6 absorbs H_2O to form the corresponding hydrate, $Li_3InCl_6{\cdot}xH_2O$, as discussed in the *operando* SXRD section. Therefore, we propose that the following reactions are taking place upon moisture exposure

$$2Li_3InCl_6 + 3H_2O \rightarrow In_2O_3(s) + 6HCl(g) + 6LiCl \quad (2)$$

$$Li_3InCl_6 + xH_2O \rightarrow Li_3InCl_6{\cdot}xH_2O \quad (3)$$

https://dx.doi.org/10.1021/acs.chemmater.0c02419
Chem. Mater. 2020, 32, 7019−7027

where HCl is produced as gas. The exact molecule structure of the corresponding hydrate, $Li_3InCl_6{\cdot}xH_2O$, has not been clarified, which need more characterization in the future.

It is interesting to note that the crystal structure of Li_3InCl_6 is similar to $InCl_3$, which is soluble in water and is stable to moisture at room temperature.[33] It is crucial to understand the mechanism that results in the instability of Li_3InCl_6 to moisture. As shown in Figure S10 (see Supporting Information), after dissolution in DI water with a weight percentage of 20 wt %, the $InCl_3$ solution remained transparent without any precipitate after having been stored for 24 h. Additionally, the *operando* Raman study of $InCl_3$ exposed to air with the 30% humidity was also carried out. During the exposure process, no peaks belonging to In_2O_3 are observed; however, some new peaks are found to increase in intensity with the exposure time. The new peaks are assigned to the corresponding hydrate $InCl_3{\cdot}4H_2O$. The reaction involving $InCl_3$ is totally different from that of Li_3InCl_6. The different reaction mechanism is due to the slight difference between crystal structures of Li_3InCl_6 and $InCl_3$. Although the crystal structures of both are very similar with the $InCl_6$ octahedra, there is only one Li^+ layer in Li_3InCl_6. The Li^+ layer is the main reason for the high ionic conductivity in Li_3InCl_6 and also might be the origin of instability to moisture, which needs to be studied in more detail in the future.

Discussion of Air Stability of Li_3InCl_6 and Its Influence on Practical Applications. As discussed above, the air stability of Li_3InCl_6 has been studied. The instability of Li_3InCl_6 to moisture makes it difficult to fabricate commercial ASSLIBs in ambient air. However, the moisture level during cell assembly in commercial settings is strictly controlled in the dry room.[34] In general, the relative humidity of a dry room is designed to be 0.5% with −40 °C dew point. Considering the humidity fluctuation during the practical manufacturing process, the humidity can be controlled in a range of 0.5−3%.[35] Although Li_3InCl_6 is not stable to air with high humidity (*e.g.* 30% used in this study), the ionic conductivity decay upon exposure to air with a low humidity degree (3−5%) is pretty slow, as shown in Figure 1E. Moreover, *ex situ* XANES was also carried out to detect the influence of low humidity (∼3%) on the chemical composition, as shown in Figure S11 (see Supporting Information). Generally, the overall features of the In L_3-edge and Cl K-edge XANES spectra have not undergone significant change after exposure to air with 3% humidity for 24 h, although the intensity of white lines subtly decrease along with a slight shift in the absorption edge. This suggests that the majority of Li_3InCl_6 is stable upon the exposure process. Additionally, the lithium-ion conductivity evolution of Li_3InCl_6 upon exposure to battery dry rooms with low dew points of −43 to −51 °C (<1% relative humidity) was studied as shown in Figure S12 (see Supporting Information). It can maintain a high ion conductivity of $\sim 0.9 \times 10^{-3}$ S cm^{-1} after exposure for 24 h compared with a pristine ionic conductivity of 1.24×10^{-3} S cm^{-1}. This finding suggests that it is promising to use this halide SSE in commercial manufacturing in a humidity-controlled battery dry room, considering the reasonably large-scale solution preparation method, high ionic conductivity, and chemical stability.[13] In the future, the large-scale ASSLIB preparation processes using Li_3InCl_6 should be evaluated in a commercial battery dry room setting.

CONCLUSIONS

In summary, we have for the first time provided a clear understanding of the air stability of the halide SSE, Li_3InCl_6, using a combination of *ex situ*, *in situ*, and *operando* characterization strategies, including optical microscopy, Raman spectroscopy, SXRD, and XANES techniques. First, the reason that the ionic conductivity of Li_3InCl_6 degrades in ambient air is because of moisture, which reacts with Li_3InCl_6 upon exposure. Additionally, the reaction process between Li_3InCl_6 and moisture has been clarified with a proposed reaction scheme. Furthermore, it is found that a part of Li_3InCl_6 decomposes to nonionically conductive In_2O_3 and LiCl along with the formation of HCl, while a majority forms the corresponding hydrate. In addition to the chemical reaction study, the influence of the air stability of Li_3InCl_6 on practical industrial application has also been discussed. Li_3InCl_6 shows much better stability in air with low humidity levels. Thus, the practical application of this electrolyte in industry is deemed to be feasible in a commercial battery dry-room setting.

ASSOCIATED CONTENT

Supporting Information

The Supporting Information is available free of charge at https://pubs.acs.org/doi/10.1021/acs.chemmater.0c02419.

Additional information and figures about *in situ* and *operando* measurement setup and additional measurement results (PDF)

AUTHOR INFORMATION

Corresponding Authors

Shangqian Zhao − *China Automotive Battery Research Institute Company Ltd, Beijing 101407, China*; Email: zhaosq@glabat.com

Tsun-Kong Sham − *Department of Chemistry and Soochow-Western Centre for Synchrotron Radiation Research, University of Western Ontario, London, Ontario N6A 5B7, Canada*; orcid.org/0000-0003-1928-6697; Phone: +1-519-661-2111 ext. 86341; Email: tsham@uwo.ca

Xueliang Sun − *Department of Mechanical and Materials Engineering, University of Western Ontario, London, Ontario N6A 5B9, Canada*; orcid.org/0000-0003-0374-1245; Phone: +1-519-661-2111 ext. 87759; Email: xsun9@uwo.ca

Authors

Weihan Li − *Department of Mechanical and Materials Engineering and Department of Chemistry and Soochow-Western Centre for Synchrotron Radiation Research, University of Western Ontario, London, Ontario N6A 5B9, Canada*

Jianwen Liang − *Department of Mechanical and Materials Engineering, University of Western Ontario, London, Ontario N6A 5B9, Canada*

Minsi Li − *Department of Mechanical and Materials Engineering and Department of Chemistry and Soochow-Western Centre for Synchrotron Radiation Research, University of Western Ontario, London, Ontario N6A 5B9, Canada*

Keegan R. Adair − *Department of Mechanical and Materials Engineering, University of Western Ontario, London, Ontario N6A 5B9, Canada*

Xiaona Li − *Department of Mechanical and Materials Engineering, University of Western Ontario, London, Ontario N6A 5B9, Canada*

Yongfeng Hu − *Canadian Light Source, Saskatoon, Saskatchewan S7N 2V3, Canada*
Qunfeng Xiao − *Canadian Light Source, Saskatoon, Saskatchewan S7N 2V3, Canada*
Renfei Feng − *Canadian Light Source, Saskatoon, Saskatchewan S7N 2V3, Canada;* orcid.org/0000-0001-8566-4161
Ruying Li − *Department of Mechanical and Materials Engineering, University of Western Ontario, London, Ontario N6A 5B9, Canada*
Li Zhang − *China Automotive Battery Research Institute Company Ltd, Beijing 101407, China*
Shigang Lu − *China Automotive Battery Research Institute Company Ltd, Beijing 101407, China*
Huan Huang − *Glabat Solid-State Battery Inc., London, Ontario N6G 4X8, Canada*

Complete contact information is available at:
https://pubs.acs.org/10.1021/acs.chemmater.0c02419

Author Contributions

[#]W.L., J.L., and M.L. contributed equally to this work.

Notes

The authors declare no competing financial interest.
All data used to generate these results are available in the main text or Supporting Information.

ACKNOWLEDGMENTS

This work was funded by the Nature Sciences and Engineering Research Council of Canada (NSERC), the Canada Research Chair Program, the Canada Foundation for Innovation (CFI), the Ontario Research Fund, the Canada Light Source (CLS) at the University of Saskatchewan, the University of Western Ontario, China Automotive Battery Research Institute Co., Ltd., and Glabat Solid-State Battery Inc. CLS was supported by CFI, NSERC, NRC, CHIR, and the University of Saskatchewan. J.L. and X.L. thank the support of Mitacs Accelerate Postdoctoral Fellowship. M.L. thanks the China Scholarship Council (CSC) for the financial support. W.L. and M.L. acknowledge the receipt of support from the CLSI Graduate and Post-Doctoral Student Travel Support Program. We also appreciate the help of the beamline scientists of PGM beamline at the Canadian Light Source, Dr. Lucia Zuin and Dr. Dongniu Wang.

REFERENCES

(1) Kato, Y.; Hori, S.; Saito, T.; Suzuki, K.; Hirayama, M.; Mitsui, A.; Yonemura, M.; Iba, H.; Kanno, R. High-power all-solid-state batteries using sulfide superionic conductors. *Nat. Energy* **2016**, *1*, 16030.
(2) Janek, J.; Zeier, W. G. A solid future for battery development. *Energy* **2016**, *1*, 16141.
(3) Gao, Z.; Sun, H.; Fu, L.; Ye, F.; Zhang, Y.; Luo, W.; Huang, Y. Promises, challenges, and recent progress of inorganic solid-state electrolytes for all-solid-state lithium batteries. *Adv. Mater.* **2018**, *30*, 1705702.
(4) Kamaya, N.; Homma, K.; Yamakawa, Y.; Hirayama, M.; Kanno, R.; Yonemura, M.; Kamiyama, T.; Kato, Y.; Hama, S.; Kawamoto, K.; Mitsui, A. A lithium superionic conductor. *Nat. Mater.* **2011**, *10*, 682.
(5) Bron, P.; Johansson, S.; Zick, K.; Schmedt auf der Günne, J.; Dehnen, S.; Roling, B. Li10SnP2S12: an affordable lithium superionic conductor. *J. Am. Chem. Soc.* **2013**, *135*, 15694−15697.
(6) Seino, Y.; Ota, T.; Takada, K.; Hayashi, A.; Tatsumisago, M. A sulphide lithium super ion conductor is superior to liquid ion conductors for use in rechargeable batteries. *Energy Environ. Sci.* **2014**, *7*, 627−631.
(7) Bernuy-Lopez, C.; Manalastas, W., Jr.; Lopez del Amo, J. M.; Aguadero, A.; Aguesse, F.; Kilner, J. A. Atmosphere controlled processing of Ga-substituted garnets for high Li-ion conductivity ceramics. *Chem. Mater.* **2014**, *26*, 3610−3617.
(8) Murugan, R.; Thangadurai, V.; Weppner, W. Fast lithium ion conduction in garnet-type Li7La3Zr2O12. *Angew. Chem., Int. Ed.* **2007**, *46*, 7778−7781.
(9) Ren, Y.; Chen, K.; Chen, R.; Liu, T.; Zhang, Y.; Nan, C.-W. Oxide electrolytes for lithium batteries. *J. Am. Ceram. Soc.* **2015**, *98*, 3603−3623.
(10) Zhang, Q.; Cao, D.; Ma, Y.; Natan, A.; Aurora, P.; Zhu, H. Sulfide-Based Solid-State Electrolytes: Synthesis, Stability, and Potential for All-Solid-State Batteries. *Adv. Mater.* **2019**, *31*, 1901131.
(11) Asano, T.; Sakai, A.; Ouchi, S.; Sakaida, M.; Miyazaki, A.; Hasegawa, S. Solid Halide Electrolytes with High Lithium-Ion Conductivity for Application in 4 V Class Bulk-Type All-Solid-State Batteries. *Adv. Mater.* **2018**, *30*, 1803075.
(12) Li, X.; Liang, J.; Luo, J.; Norouzi Banis, M.; Wang, C.; Li, W.; Deng, S.; Yu, C.; Zhao, F.; Hu, Y.; Sham, T.-K.; Zhang, L.; Zhao, S.; Lu, S.; Huang, H.; Li, R.; Adair, K. R.; Sun, X. Air-stable Li 3 InCl 6 electrolyte with high voltage compatibility for all-solid-state batteries. *Energy Environ. Sci.* **2019**, *12*, 2665−2671.
(13) Li, X.; Liang, J.; Chen, N.; Luo, J.; Adair, K. R.; Wang, C.; Banis, M. N.; Sham, T. K.; Zhang, L.; Zhao, S.; Lu, S.; Huang, H.; Li, R.; Sun, X. Water-Mediated Synthesis of a Superionic Halide Solid Electrolyte. *Angew. Chem., Int. Ed.* **2019**, *58*, 16427−16432.
(14) Wang, S.; Bai, Q.; Nolan, A. M.; Liu, Y.; Gong, S.; Sun, Q.; Mo, Y. Lithium Chlorides and Bromides as Promising Solid-State Chemistries for Fast Ion Conductors with Good Electrochemical Stability. *Angew. Chem., Int. Ed.* **2019**, *58*, 8039−8043.
(15) Sahu, G.; Lin, Z.; Li, J.; Liu, Z.; Dudney, N.; Liang, C. Air-stable, high-conduction solid electrolytes of arsenic-substituted Li 4 SnS 4. *Energy Environ. Sci.* **2014**, *7*, 1053−1058.
(16) Wang, Y.; Lai, W. Phase transition in lithium garnet oxide ionic conductors Li7La3Zr2O12: The role of Ta substitution and H2O/CO2 exposure. *J. Power Sources* **2015**, *275*, 612−620.
(17) Muramatsu, H.; Hayashi, A.; Ohtomo, T.; Hama, S.; Tatsumisago, M. Structural change of Li2S−P2S5 sulfide solid electrolytes in the atmosphere. *Solid State Ionics* **2011**, *182*, 116−119.
(18) Wang, W.-G.; Wang, X.-P.; Gao, Y.-X.; Yang, J.-F.; Fang, Q.-F. Investigation on the stability of Li 5 La 3 Ta 2 O 12 lithium ionic conductors in humid environment. *Front. Mater. Sci. China* **2010**, *4*, 189−192.
(19) Liu, H.; Strobridge, F. C.; Borkiewicz, O. J.; Wiaderek, K. M.; Chapman, K. W.; Chupas, P. J.; Grey, C. P. Capturing metastable structures during high-rate cycling of LiFePO4 nanoparticle electrodes. *Science* **2014**, *344*, 1252817.
(20) Li, W.; Li, M.; Hu, Y.; Lu, J.; Lushington, A.; Li, R.; Wu, T.; Sham, T.-K.; Sun, X. Synchrotron-Based X-ray Absorption Fine Structures, X-ray Diffraction, and X-ray Microscopy Techniques Applied in the Study of Lithium Secondary Batteries. *Small Methods* **2018**, *2*, 1700341.
(21) Lin, F.; Liu, Y.; Yu, X.; Cheng, L.; Singer, A.; Shpyrko, O. G.; Xin, H. L.; Tamura, N.; Tian, C.; Weng, T.-C.; Yang, X.-Q.; Meng, Y. S.; Nordlund, D.; Yang, W.; Doeff, M. M. Synchrotron X-ray analytical techniques for studying materials electrochemistry in rechargeable batteries. *Chem. Rev.* **2017**, *117*, 13123−13186.
(22) Bak, S.-M.; Shadike, Z.; Lin, R.; Yu, X.; Yang, X.-Q. In situ/operando synchrotron-based X-ray techniques for lithium-ion battery research. *NPG Asia Mater.* **2018**, *10*, 563−580.
(23) Wang, Y.; Richards, W. D.; Ong, S. P.; Miara, L. J.; Kim, J. C.; Mo, Y.; Ceder, G. Design principles for solid-state lithium superionic conductors. *Nat. Mater.* **2015**, *14*, 1026−1031.
(24) Bertie, J. E.; Michaelian, K. H.; Eysel, H. H.; Hager, D. The Raman-active O−H and O−D stretching vibrations and Raman spectra of gaseous formic acid-d 1 and-OD. *J. Chem. Phys.* **1986**, *85*, 4779−4789.
(25) Torii, H. Time-domain calculations of the polarized Raman spectra, the transient infrared absorption anisotropy, and the extent of

delocalization of the OH stretching mode of liquid water. *J. Phys. Chem. A* **2006**, *110*, 9469−9477.
(26) Chen, H.-C.; Lin, H.-C.; Chen, H.-H.; Mai, F.-D.; Liu, Y.-C.; Lin, C.-M.; Chang, C.-C.; Tsai, H.-Y.; Yang, C.-P. Innovative strategy with potential to increase hemodialysis efficiency and safety. *Sci. Rep.* **2015**, *4*, 4425.
(27) Tsuji, J.; Nakamatsu, H.; Mukoyama, T.; Kojima, K.; Ikeda, S.; Taniguchi, K. Lithium K-edge XANES spectra for lithium compounds. *X Ray Spectrom.* **2002**, *31*, 319−326.
(28) Tsuji, J.; Kojima, K.; Ikeda, S.; Nakamatsu, H.; Mukoyama, T.; Taniguchi, K. Li K-edge spectra of lithium halides. *J. Synchrotron Radiat.* **2001**, *8*, 554−556.
(29) Sham, T. K. L-edge x-ray-absorption systematics of the noble metals Rh, Pd, and Ag and the main-group metals In and Sn: A study of the unoccupied density of states in 4d elements. *Phys. Rev. B* **1985**, *31*, 1888.
(30) Marezio, M. Refinement of the crystal structure of In2O3 at two wavelengths. *Acta Crystallogr.* **1966**, *20*, 723−728.
(31) Hedman, B.; Hodgson, K. O.; Solomon, E. I. X-ray absorption edge spectroscopy of ligands bound to open-shell metal ions: chlorine K-edge studies of covalency in tetrachlorocuprate (2-). *J. Am. Chem. Soc.* **1990**, *112*, 1643−1645.
(32) Rompel, A.; Andrews, J. C.; Cinco, R. M.; Wemple, M. W.; Christou, G.; Law, N. A.; Pecoraro, V. L.; Sauer, K.; Yachandra, V. K.; Klein, M. P. Chlorine K-edge X-ray absorption spectroscopy as a probe of chlorine− manganese bonding: model systems with relevance to the oxygen evolving complex in photosystem II. *J. Am. Chem. Soc.* **1997**, *119*, 4465−4470.
(33) Asikainen, T.; Ritala, M.; Leskelä, M. Growth of In2 O 3 Thin Films by Atomic Layer Epitaxy. *J. Electrochem. Soc.* **1994**, *141*, 3210.
(34) Maiser, E. Battery packaging-Technology review. *AIP Conference Proceedings*, 2014; Vol. *1597*, pp 204−218.
(35) Ahmed, S.; Nelson, P. A.; Dees, D. W. Study of a dry room in a battery manufacturing plant using a process model. *J. Power Sources* **2016**, *326*, 490−497.

https://dx.doi.org/10.1021/acs.chemmater.0c02419
Chem. Mater. 2020, 32, 7019−7027